

**Subcontract XAT-4-33624-01**

**“Development of a Wide Band Gap Cell for Thin Film Tandem Solar Cells”**

**2nd Quarterly Report**

**to**

**National Renewable Energy Laboratory**

**From**

**Institute of Energy Conversion  
University of Delaware**

**For period 2/6/04 - 5/5/04**

**Task 1: I-III-VI<sub>2</sub>-based Solar Cells**

*Cu(InGa)(SeS)<sub>2</sub> Film Growth*

Much of the work this quarter continued to focus on the relative incorporation of S and Se during CuIn(SeS)<sub>2</sub> or Cu(InGa)(SeS)<sub>2</sub> deposition. In the previous quarterly report, we showed that there was a reproducible difference between films grown with Cu-rich composition and those with Cu-poor composition. Films deposited with  $\text{Cu}/(\text{In}+\text{Ga}) > 1.1$  preferentially incorporate S, while those with  $\text{Cu}/(\text{In}+\text{Ga}) < 0.9$  preferentially incorporate Se. This is shown in Figure 1, which plots the relative S and Se incorporation in films, as measured by EDS, as a function of the  $\text{S}/(\text{S}+\text{Se})$  ratio in the vapor, determined by the average effusion rate measured for each source during the run. For both the Cu-rich and Cu-poor cases, there is no correlation with  $\text{Ga}/(\text{In}+\text{Ga})$  and data is included for CuIn(SeS)<sub>2</sub> films as well as Cu(InGa)(SeS)<sub>2</sub> with different  $\text{Ga}/(\text{In}+\text{Ga})$ . Post-deposition KCN etching, to remove a surface  $\text{Cu}_x(\text{SeS})_y$  layer typically lowers  $\text{S}/(\text{Se}+\text{S})$  in the film a small amount, as demonstrated for one sample.

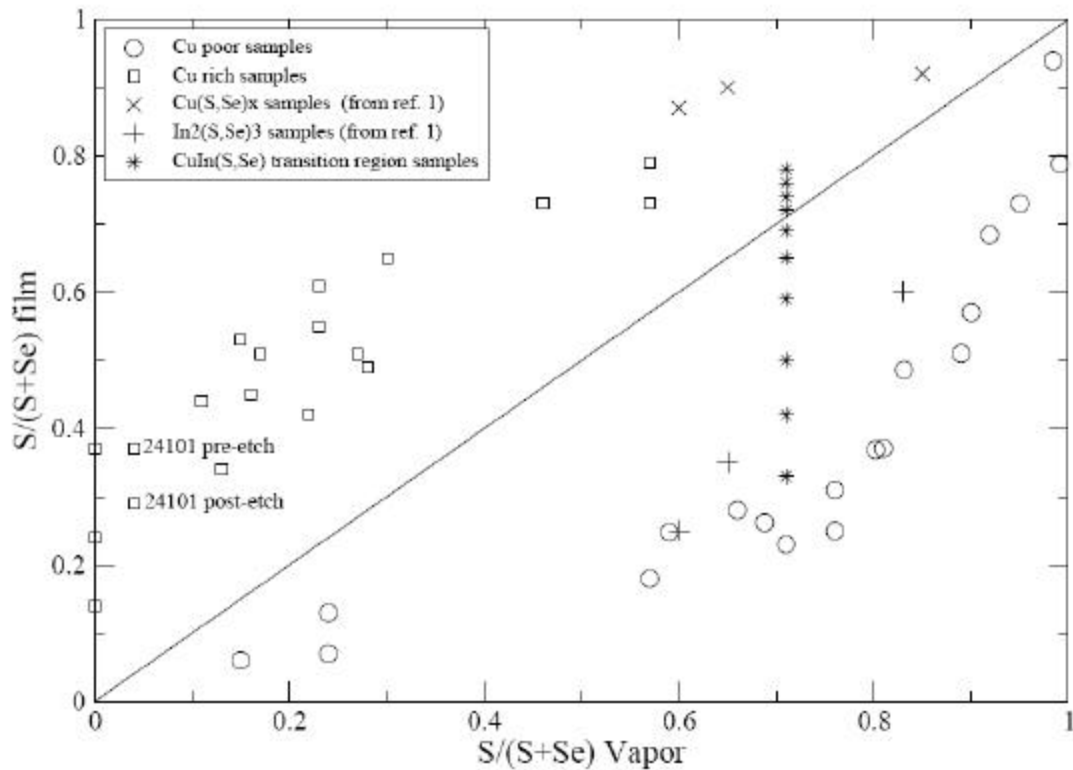


Figure 1. Relative S content,  $S/(S+Se)$ , in  $Cu(InGa)(SeS)_2$  films as a function of the relative S flux for films grown with Cu-poor or Cu-rich composition. Also shown are films (\*) with  $Cu/(In+Ga)$  ratio nearly equal to 1, as well as data from a previous paper by Walter *et al* [1].

The data points on the y axis of the plot represent films grown without intentional S evaporation. S in the film must be due to residual S in the chamber.  $S/(S +Se)$  in these as-grown films varied from 0.14 to 0.37. There is also variability in S incorporation at other points on the x-axis for both Cu-rich and Cu-poor samples. This variability does not correlate with variation in  $(S+Se)/(Cu+In+Ga)$  effusion rates, nor with  $Cu/(In+Ga)$  or  $Ga/(In+Ga)$  in the film. Although some of the variability represents the inherent measurement errors, it is concluded that the amount of residual S in the chamber varies from run to run, which is an undesirable situation.

Further evidence that the amount of deviation from the diagonal line in Figure 1 is usually not correlated to the  $Cu/(In+Ga)$  is the data for  $In_2(SeS)_3$  and  $Cu_x(SeS)_y$  from Reference 1. These data points in the figure fall in the same range as the films grown at IEC. In other words, films grown infinitely Cu-rich or Cu-poor agree with the IEC data where  $Cu/(In+Ga)$  varied from roughly 0.5 to 2.0. Growth conditions in Reference 1 were not stated clearly and may differ somewhat from IEC growth conditions.

The major theme of Figure 1 is that a very small change in  $Cu/(In+Ga)$ ; i.e., from slightly less than 1 (Cu poor) to slightly greater than 1 (Cu rich), leads to a large change in  $S/(S+Se)$  in the film for a given  $S/(S+Se)$  in the vapor. Films have also been grown to

span the transition point between Cu-poor and Cu-rich in a single run in which there was a gradient in relative Cu flux across the array of substrates. This resulted in a variation in Cu/(In+Ga) as shown by a representative sampling of data in Figure 1 as a series of asterisks which line up vertically. It is not easy to determine the flux at different points on the substrate plane so the points are all shown with the same S/(S+Se) vapor ratio of 0.71, as determined by the effusion rate from the source.

Figure 2 shows a more complete set of EDS data points from this run. It is apparent that there is a steep gradient in S/(Se+S) for  $0.92 = \text{Cu}/(\text{In}+\text{Ga}) = 1.02$  while outside this range of Cu/(In+Ga) there is only a small effect on the S/(S+Se) ratio. Further analysis of these near-stoichiometric films may yield clues as to factors which control chalcogen element incorporation and the growth mechanism in general.

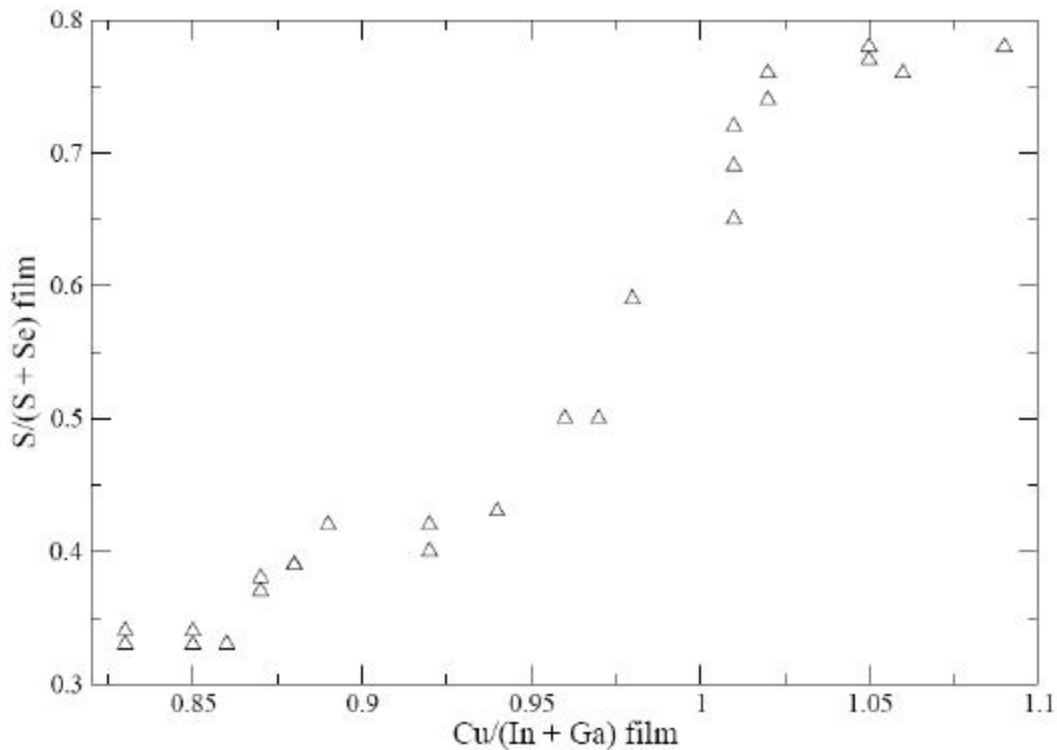


Figure 2. S/(S+Se) versus Cu/(In+Ga) at different spots in the films of run 24133. The S/(S+Se) in the vapor was 0.71 as determined by effusion rates.

Cu-rich films are expected to have a bi-layer structure with a layer of  $\text{Cu}_x(\text{SeS})_y$  on top of stoichiometric  $\text{Cu}(\text{InGa})(\text{SeS})_2$ . EDS measurements only measure an average composition over the top  $\sim 1 \mu\text{m}$  of the composite film. Further characterization was done by XRD in both symmetric and glancing incident angle (GIXRD) measurements to determine what phases are present before and after etching with KCN. Symmetric XRD on Cu-rich sample 24101-11 only showed  $\text{Cu}(\text{InGa})(\text{SeS})_2$  chalcopyrite peaks in both cases. GIXRD spectra are shown in Figure 2. Before the etch, several peaks (labeled 2, 3, and 4 in the figure) were present that were not present after the etch. The peak positions and intensities indicate that the surface layer is a CuS phase.

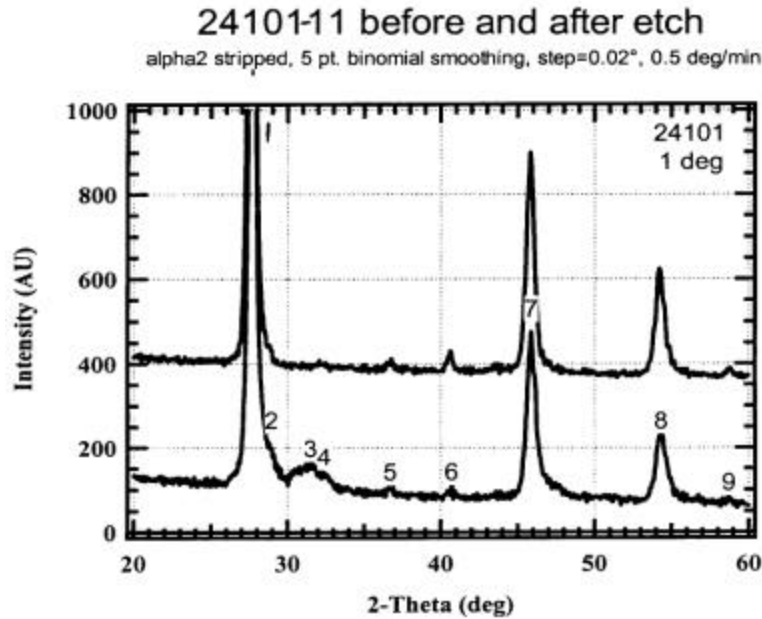


Figure 3. GIXRD scans for a Cu-rich CIGSS film before (bottom spectrum) and after (top) a KCN etch.

In an attempt to corroborate and go beyond the EDS and XRD results, Auger depth profiling was done on the same sample. It should be pointed out that we are presently attempting to calibrate and standardize both sputtering depth and atomic percentage, so the Auger data is presented qualitatively rather than quantitatively. Before etching, sulfur predominates at the surface. Likewise, the Cu/(In+Ga) ratio is much larger at the surface than in the bulk. After KCN etching this sample, the Cu/(In+Ga) ratio tends toward 1 in the bulk. Copper is actually somewhat depleted at this new surface. KCN acts to complex Cu ions, so perhaps Cu is being removed from the chalcopyrite phase slowly and to a small extent, near the surface. Finally, S is still predominant at the surface of the post-etch film, though this layer of enrichment is much thinner than the pre-etch S enrichment layer. Solvated S ions may diffuse into the film during the etch. Further investigation is underway to understand these post-etch phenomena.

### *Cu(InGa)(SeS)<sub>2</sub> Devices*

In previous reports, we have presented Cu(InGa)(SeS)<sub>2</sub> device results with fixed bandgap  $E_g \sim 1.5$  eV but varying Ga/(In+Ga) and S/(Se+S), using films deposited either Cu-poor or Cu-rich with a post-deposition KCN etch. In the Cu-poor case, the best device efficiency was attained with the Cu(InGa)Se<sub>2</sub> absorber that contained no S and in the Cu-rich case, the best device was with the CuInS<sub>2</sub> absorber that contained no Ga or Se.

Table 1 shows the J-V parameters for a CuInS<sub>2</sub> device (deposited Cu-rich) and a Cu(InGa)Se<sub>2</sub> device (deposited Cu-poor) which have comparable efficiency. The

Cu(InGa)Se<sub>2</sub> device has significantly higher V<sub>oc</sub> but lower J<sub>sc</sub> and FF. Further analysis is underway to quantify the differences. QE curves, plotted in Figure 4, show a distinct difference between the 2 devices. The CuInSe<sub>2</sub> device is shown only at 0V, and there was no change with reverse voltage bias, indicating little loss due to voltage dependent current collection. The Cu(InGa)Se<sub>2</sub> device, on the other hand, showed increased collection with reverse voltage bias which could cause reduced J<sub>sc</sub> and FF.

To determine if the differences in QE might also be related to difference in optical absorption, the optical constants of CuInSe<sub>2</sub> are being determined from spectroscopic ellipsometry measurements and will be compared to Cu(InGa)Se<sub>2</sub> with comparable bandgap. Additional device analysis which might help understand the difference in V<sub>oc</sub> will be done after more CuInSe<sub>2</sub> devices are fabricated, since the device shown developed a shunt after a short annealing treatment.

Table 1. J-V parameters of Cu(InGa)Se<sub>2</sub> (Cu-poor deposition) and CuInS<sub>2</sub> (Cu-rich deposition) devices with no AR layers.

Absorber	$\eta$ (%)	V <sub>oc</sub> (V)	J <sub>sc</sub> (mA/cm <sup>2</sup> )	FF (%)
Cu(InGa)Se <sub>2</sub>	9.2	0.826	17.7	62.2
CuInS <sub>2</sub>	8.9	0.643	20.6	67.6

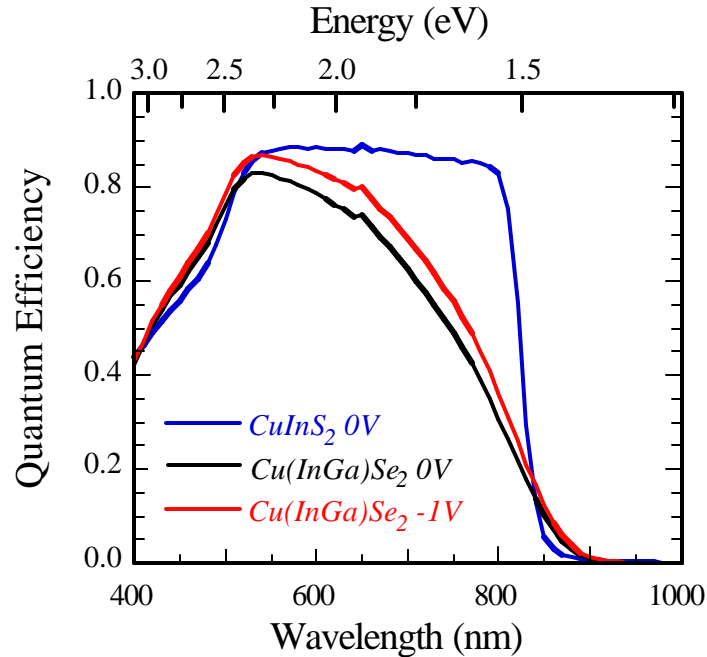


Figure 4. QE curves for Cu(InGa)Se<sub>2</sub> (Cu-poor deposition) and CuInS<sub>2</sub> (Cu-rich deposition) devices.

## Task 2. II-VI-based Solar Cells

Research during this quarter focused on analysis of interfacial reactivity in  $\text{Cd}_{1-x}\text{Zn}_x\text{Te}/\text{CdS}$  device structures to determine the phase composition after thermo-chemical processing. As previously reported, the best  $\text{Cd}_{1-x}\text{Zn}_x\text{Te}/\text{CdS}$  devices with  $x > 0.1$  and processed with high temperature anneal and heat treatments in  $\text{ZnCl}_2$  vapor exhibit low performance with  $J_{sc}$  2-3X lower than expected for the band gap and no increase in  $V_{oc}$ . The low current is attributed to poor collection instead of generation since it improves with voltage bias. Further, it is likely limited at the heterojunction or front contact since the device behavior is insensitive to back contact processing. This could arise either from a thin defective layer between the CdS and  $\text{Cd}_{1-x}\text{Zn}_x\text{Te}$  or from poor conduction band alignment, resulting in a barrier to electron transport across the junction. The experimental approach to understanding the collection problem from a materials perspective consists of two types of experiments: 1) ascertain the chemical stability between CdS and the  $\text{Cd}_{1-x}\text{Zn}_x\text{Te}$  alloy and 2) evaluate the effect of different window layers on current collection in cells with  $\text{Cd}_{1-x}\text{Zn}_x\text{Te}$  layers having different Zn content.

### *CdS-CdZnTe interface chemistry*

In  $\text{Cd}_{1-x}\text{Zn}_x\text{Te}/\text{CdS}$  devices, diffusion across the interface is expected to occur during processing. In addition, the affinity of Zn for both S and O, compared to Cd, may be the dominant component in the Cd-Zn-Te-S-O system.

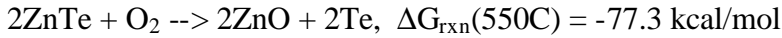
Diffusion of CdS into the  $\text{Cd}_{1-x}\text{Zn}_x\text{Te}$  layer might either produce a quaternary  $\text{Cd}_{1-x}\text{Zn}_x\text{Te}_{1-y}\text{S}_y$  alloy or result in an exchange of components, forming a multiphase system. The existence of the quaternary  $\text{Cd}_{1-x}\text{Zn}_x\text{Te}_{1-y}\text{S}_y$  alloy over a limited compositional range has been demonstrated in thin-film form when produced by sublimation from sintered targets onto glass at room temperature [2]. Considering the quaternary as a pseudo-binary system between  $\text{CdTe}_{1-y}\text{S}_y$  and  $\text{ZnTe}_{1-y}\text{S}_y$ , in which wide miscibility gaps have been established ( $\text{CdTe}_{1-y}\text{S}_y$ ) [3] or demonstrated ( $\text{ZnTe}_{1-y}\text{S}_y$ ) [4], leads to the expectation of a wide miscibility gap in the quaternary  $\text{Cd}_{1-x}\text{Zn}_x\text{Te}_{1-y}\text{S}_y$  system. Furthermore, the Gibbs phase rule, applied to 4 components and 2 degrees of freedom (T, P), allows for 4 co-existing phases on the  $T_{-x,-y}$  projection of the quaternary system.

To understand how these considerations apply to the thin-film solar cell we are trying to develop, we are conducting materials-related experiments along three paths:

1. Investigate ZnTe-CdS interdiffusion using ZnTe/CdS film couples deposited by sequential evaporation CdS and ZnTe onto ITO coated 7059 glass.
2. Determine the miscibility gap and characteristic diffusion times in the  $\text{ZnTe}_{1-y}\text{S}_y$  system using  $\text{ZnTe}_{1-y}\text{S}_y$  films deposited by co-evaporation of ZnTe and ZnS onto ITO coated 7059 glass.
3. Determine the stable phases in the  $\text{Cd}_{1-x}\text{Zn}_x\text{Te}_{1-y}\text{S}_y$  system using  $\text{Cd}_{1-x}\text{Zn}_x\text{Te}_{1-y}\text{S}_y$  films deposited by co-evaporation of ZnTe and CdS onto ITO coated 7059 glass.

In each case, the films are analyzed for chemical composition by EDS and crystalline phase content by XRD. Interpretation of the XRD patterns and line profiles is carried out according to procedures established for investigation of the CdTe-CdS system [5]. In this report, XRD data is shown in the as-deposited state and after thermal treatment at 550°C for 30 minutes, which corresponds to the highest temperature used to process Cd<sub>1-x</sub>Zn<sub>x</sub>Te/CdS cells. The raw XRD plots are shown and the quantitative results are summarized below.

For ZnTe/CdS, shown in Figures 5 and 6, all peaks in the as-deposited condition are indexed as CdS, ZnTe and In<sub>2</sub>O<sub>3</sub> (ITO). The reflections are sharp, following Pearson VII functional form with a shape parameter of ~3, indicating good crystal quality and no lattice distortion. The 550°C treatment was carried out in two atmospheres: argon and 4% hydrogen in 96% argon. The treatment in flowing argon resulted in a darkening of the end of the quartz treatment tube liner and a visible lightening of the sample appearance. EDS analysis of the dark tube deposits indicated nearly pure Te, while XRD analysis of the film indicated formation of ZnO. Furthermore, the CdS lattice parameters increased while the ZnTe peaks broadened towards larger lattice parameter. From this, it is concluded that residual oxygen in the treatment tube reacted with the ZnTe film, forming ZnO and releasing volatile Te according to the favored reaction:



Accordingly, a second experiment was carried out in reducing ambient to minimize the effects of residual oxygen (Figure 2). In this experiment, there were no additional phases formed and no change in either CdS or ZnTe reflections, indicating that the ZnTe/CdS couple did not detectably interact during the 550°C treatment. Treatments will be carried out in ZnCl<sub>2</sub> vapor at 400°C, corresponding to cell fabrication conditions, which is expected to enhance grain boundary diffusivity.

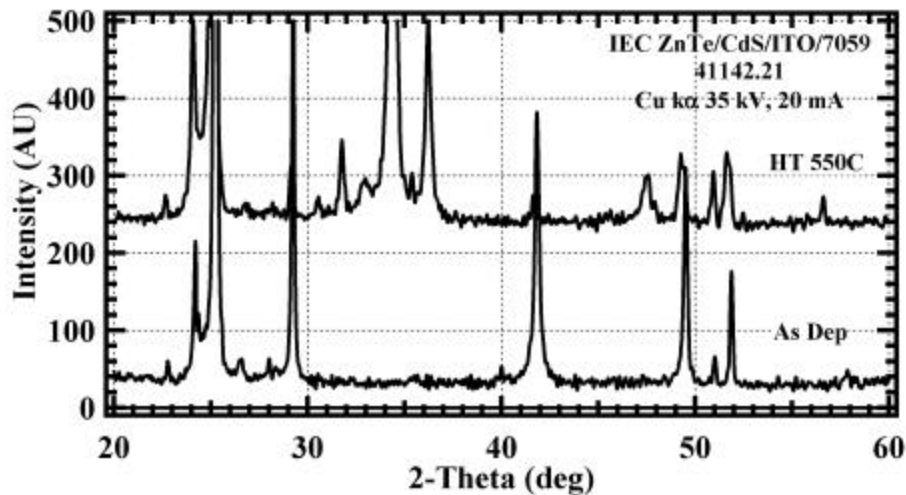


Figure 4. XRD of ZnTe/CdS couple: as deposited and after 550°C HT in Ar (residual O<sub>2</sub>)

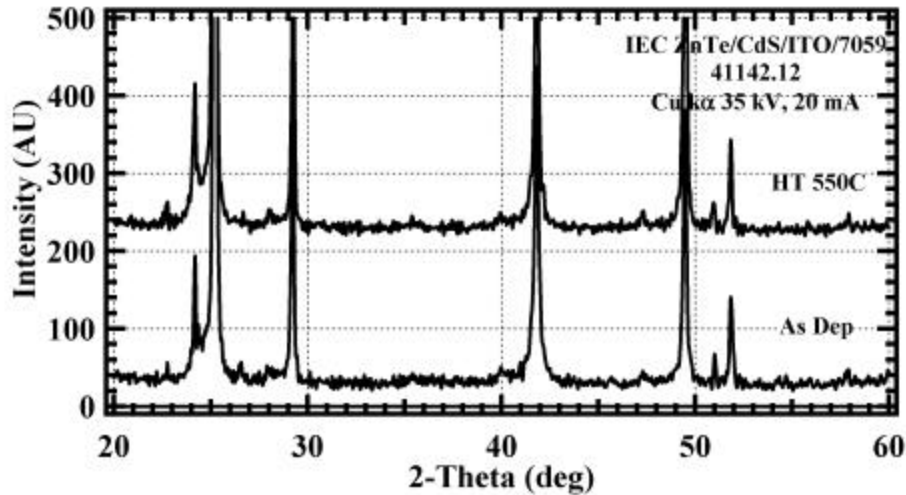


Figure 5. XRD of ZnTe/CdS couple: as deposited and after 550°C HT in 4% H<sub>2</sub>:Ar

To investigate the ZnTe<sub>1-y</sub>S<sub>y</sub> system, a deposition was carried out onto nine ITO-coated 7059 substrates by co-evaporating ZnTe and ZnS to form the alloy. The sources were held at 1020°C (ZnS) and 805°C (ZnTe) and deposition was carried out at a substrate temperature of 200°C. EDS composition of the films was Zn (51%) Te (31%) and S (18%), corresponding to an approximate alloy composition of ZnTe<sub>0.6</sub>S<sub>0.4</sub>, which is near the middle of the pseudobinary range and is thus suitable for evaluating the miscibility gap. The as-deposited or treated film, however, cannot be treated as single phase as shown in the XRD pattern (Figure 6). The patterns exhibit sharp peaks corresponding to In<sub>2</sub>O<sub>3</sub> (ITO) and broad peaks corresponding to the approximate locations for (111), (220) and (311) reflections of a zincblende structure with a lattice parameter range centered on ~5.8 Å. Although this is close to the value of 5.66 Å expected for the EDS composition, the reflections are broad. Furthermore, the (111) and (311) reflections exhibit bimodal shape, indicating the presence of two discrete alloy compositions in the film. The heat treatment sharpened the reflections slightly but did not change their locations, suggesting that the sample may already be near its equilibrium state. The doublet separation yields lattice parameters of 5.87 Å and 5.74 Å, corresponding to ZnTe<sub>0.66</sub>S<sub>0.34</sub> and ZnTe<sub>0.48</sub>S<sub>0.51</sub>.

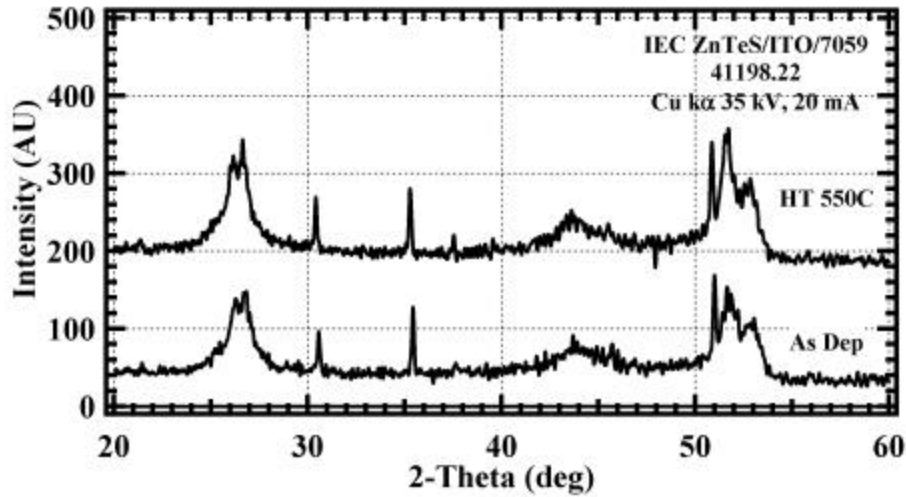


Figure 6. XRD of ZnTeS/ITO: as deposited and after 550°C HT in pure Ar.

Based on published bowing parameters for the ZnTe-ZnS system, the alloys of Figure 6 would have optical band gaps of 2.5 and 2.2 eV. The optical transmission of the film shows a sharp band edge with 90% sub-band gap transmission (Figure 7). Analysis of the film transmission edge, by assuming a direct transition and extrapolating on a plot of  $\alpha^2$  versus E, gives an optical band gap of 2.1 eV, which is only 0.1 eV lower than that expected for the ZnTe<sub>0.48</sub>S<sub>0.51</sub> alloy. As a preliminary result, this data shows that a range of ZnTe-ZnS alloys exist and are stable at the cell processing temperature. As above, this experiment will be repeated in kinetic-enhancing ambient (ZnCl<sub>2</sub>) to determine the endpoint for stability at the processing temperatures used to fabricate cells.

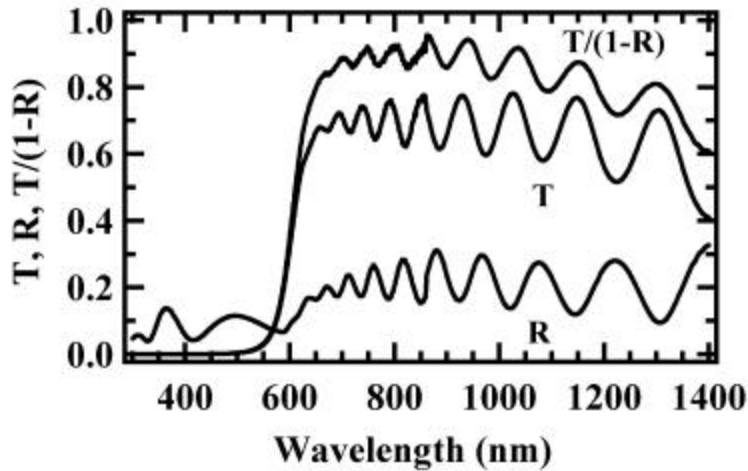


Figure 7. Optical transmission, reflection and normalized transmission,  $T/(1-R)$ , of ZnTe<sub>1-y</sub>S<sub>y</sub> deposited on ITO/7059.

To investigate the existence and stability in the quaternary Cd<sub>1-x</sub>Zn<sub>x</sub>Te<sub>1-y</sub>S<sub>y</sub> system, a deposition was carried out onto nine ITO-coated 7059 substrates by co-evaporating ZnTe and CdS to form the alloy. The sources were held at 825°C (ZnTe) and 825°C (CdS) and deposition was carried out at a substrate temperature of 200°C. EDS composition of the

films was Cd (28%) Zn (23%) Te (32%) and S (17%), corresponding to an approximate alloy composition of  $(\text{Cd}_{0.55}\text{Zn}_{0.45})(\text{Te}_{0.65}\text{S}_{0.35})$ , which is a suitable starting point for evaluating the stable phases. As shown in Figure 8, the as-deposited film exhibits a single sharp reflection near  $2\theta = 25^\circ$  corresponding to the closest packing of zincblende (111) or wurtzite (002). A broad feature is also found in the range expected for zincblende (220) and (311) reflections. This suggests that with respect to the plane of the substrate, reasonable long-range order is only found for grains having the  $\langle 111 \rangle$  closest-packing direction, while the remainder of the film is disordered. The patterns also exhibit minor peaks corresponding to  $\text{In}_2\text{O}_3$  (ITO) from the substrate. The heat treatment at  $550^\circ\text{C}$  in argon eliminated the initial alloy reflections and produced a new set of sharp reflections which are interpreted as belonging to the zincblende structure  $\text{CdTe}_{1-x}\text{S}_x$  and  $\text{ZnS}_{1-x}\text{Te}_x$  alloys. For the  $\text{CdTe}_{1-x}\text{S}_x$  phase, 8 reflections were found on scans from  $2\theta = 20$ - $90^\circ$ , from which a zincblende lattice parameter of 6.449 Å, corresponding to  $\text{CdTe}_{0.952}\text{S}_{0.048}$ , was determined using the Nelson-Riley-Sinclair-Taylor method. Only 2 reflections were found of the second phase, and these yield a lattice parameter of 5.44 Å, corresponding to  $\text{ZnS}_{0.96}\text{Te}_{0.04}$ . This experiment suggests that the quaternary  $\text{Cd}_{1-x}\text{Zn}_x\text{Te}_{1-y}\text{S}_y$  system is only metastable and probably would not form spontaneously by thermal diffusion of species across the boundary between  $\text{Cd}_{1-x}\text{Zn}_x\text{Te}$  and  $\text{CdS}$ .

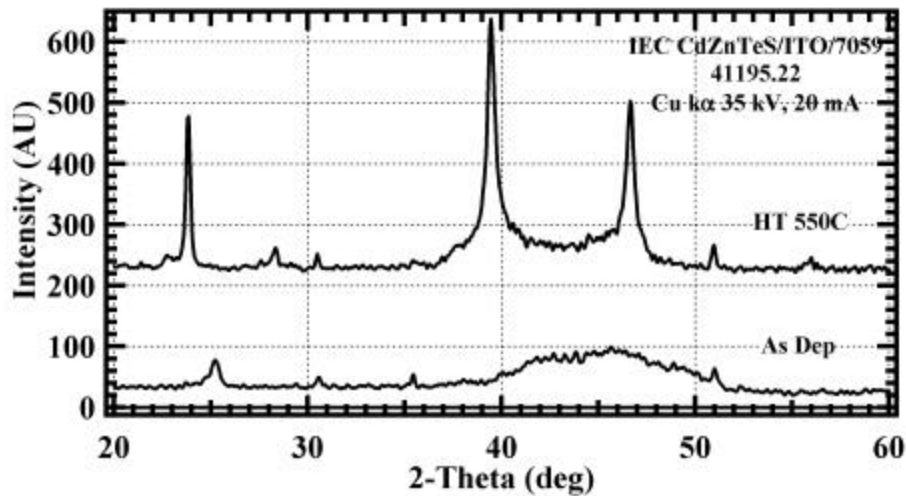


Figure 8. XRD of  $\text{Cd}_{1-x}\text{Zn}_x\text{Te}_{1-y}\text{S}_y/\text{ITO}$ : as deposited and after  $550^\circ\text{C}$  HT in pure Ar.

In summary, we have found that for thermal treatment at  $550^\circ\text{C}$ , ZnTe/CdS couples are extremely sensitive to residual oxygen, owing to the high reactivity of ZnTe; and when oxygen is present, ZnO is produced by conversion of the ZnTe and Te is evolved into the treatment vessel. For treatment in reducing ambient, no changes were detected in phase composition and no evidence for interdiffusion was detected. This, taken with the good crystallinity found for both pure ZnTe and pure CdTe films, implies that bulk diffusion coefficient for CdS into ZnTe is low. For structures with  $\text{Cd}_{1-x}\text{Zn}_x\text{Te}$ , however, disorder in the grains of the alloy film may raise the bulk diffusivity and lead to chemical change at the interface. The ternary  $\text{ZnTe}_{1-y}\text{S}_y$  system appears to be thermally stable for mid-range compositions and a miscibility gap may exist near the mid-range. The quaternary  $\text{Cd}_{1-x}\text{Zn}_x\text{Te}_{1-y}\text{S}_y$  system appears to be metastable for mid-range compositions, segregating

into  $\text{CdTe}_{1-x}\text{S}_x$  and  $\text{ZnS}_{1-x}\text{Te}_x$  ternary alloys. This suggests that the diffusion of CdS into  $\text{Cd}_{1-x}\text{Zn}_x\text{Te}$  creates an unstable four-element system, promoting decomposition of the original alloy absorber layer into a mixed phase region at the interface, consisting of a disordered layer of  $\text{CdTe}_{1-x}\text{S}_x$  and  $\text{ZnS}_{1-x}\text{Te}_x$ . An approach for overcoming this tendency is to reduce the diffusion driving force, by incorporating Zn at comparable levels on both sides of the junction. The anion components will still be the driving force for interdiffusion (S into the absorber and Te into the window), but the presence of a high proportion of Zn-S bonds in the window could retard lattice decomposition.

### *Device fabrication*

We have deposited  $\text{Cd}_{1-x}\text{Zn}_x\text{S}$  films by chemical surface deposition [6] on ITO-coated 7059 glass for use as window layers in  $\text{Cd}_{1-x}\text{Zn}_x\text{Te}/\text{Cd}_{1-x}\text{Zn}_x\text{S}$  solar cells. The deposition method consists of applying a solution containing  $\text{Cd}^{++}$ ,  $\text{Zn}^{++}$ , thiourea and ammonia onto preheated superstrates for 3-5 minutes. Heat for the reaction is obtained from the superstrate surface, resulting in heterogeneous nucleation with uniform, conformal film growth and high utilization of Cd species. For the first set of samples, the proportion of  $\text{Zn}^{++}$  added to the solution was increased, while all other constituent concentrations were held constant. Optical transmission measurements showed that the transmission edge is progressively shifted to shorter wavelength as the quantity of  $\text{Zn}^{++}$  added to the solution was increased. In addition, the thickness decreased. Similar samples are being fabricated to be used in devices with  $\text{Cd}_{1-x}\text{Zn}_x\text{Te}$  absorber layers.

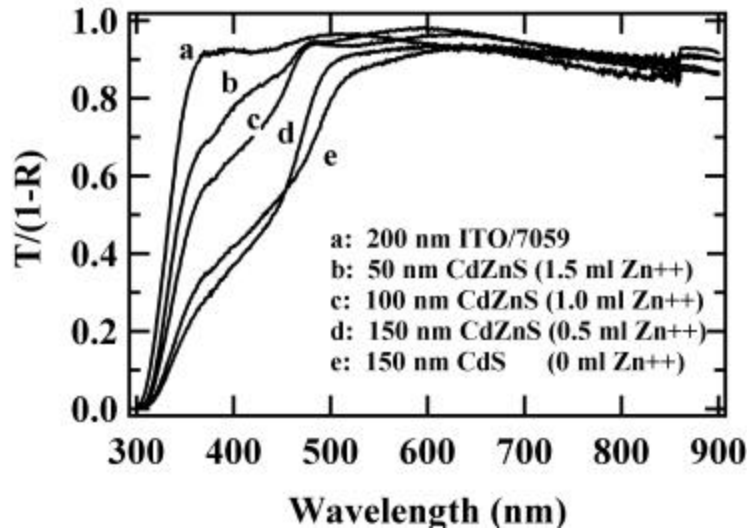


Figure 9. Optical transmission,  $T/(1-R)$ , of  $\text{Cd}_{1-x}\text{Zn}_x\text{S}$  window layers on ITO/7059 substrates.

### Task 3. Collaboration

Cu(InGa)Se<sub>2</sub> films were deposited simultaneously on glass/Mo and glass substrates for experiments at the U. of Oregon. These will be used to enable cross-grain electrical measurements on the insulating substrate for comparison to the mobility determined from high frequency freeze-out of the admittance.

### References

1. T. Walter, M. Ruckh, K.O. Velthaus, and H.W. Schock, 11th EC Photovoltaic Solar Energy Conference, Montreux. (1992) 124-7.
- 2 N. Lakshmi, N. Madhusudhana Rao, R. Venugopal, D. R. Reddy, B. K. Reddy, *Materials Chemistry and Physics* 82 (2003) 764-770.
- 3 B. E. McCandless, G. M. Hanket, D. G. Jensen, R. W. Birkmire, *J. Vac. Sci. Technol. A* 20(4) (2002) 1462-1467.
- 4 S. Larach, R. E. Shrader, C. F. Stocker, *Phys. Rev.* 108(3) (1957) 587-589.
- 5 B. E. McCandless, M. G. Engelmann, R. W. Birkmire, "Interdiffusion of CdS/CdTe thin films: modeling x-ray diffraction line profiles," *J. Appl. Phys.* 89(2) (2001) 988-994.
- 6 B. E. McCandless and W. N. Shafarman, *Conf. Rec. 3<sup>rd</sup> WCPEC* (2003)